Energy flux to the substrate in a magnetron discharge with hollow cathode

N P Poluektov, Yu P Tsar'gorodsev, I I Usatov, A G Evstigneev,

Department of Physics, Mytishchi branch of Bauman Moscow State Technical University

141005 Mytischi-5, Moscow Region, Russia

E-mail: poluekt@mgul.ac.ru

ABSRACT

The energy flux to the substrate was measured in a hollow cathode magnetron (HCM) discharge. Feature of this discharge is high density plasma created in a large volume. The measurements of energy flux at different pressures and distances from the target are presented. As a result, at a distance greater than 20 cm from the target flux density is equal to hundreds mW/cm^2 for DC power supply of 2.1 kW. The energy flux increases linearly with discharge power and depends strongly on magnetic field geometry. Langmuir probe was used to study the spatial distribution of plasma parameters such as the electron density and temperature, plasma space and floating potentials. The temperature of Cu and Ar atoms and a deposition rate were measured with a Fabry-Perot interferometer and a quartz crystal microbalance respectively. Using data obtained the contributions from charged and neutral species to the total power density were determined. Comparison of the measured and calculated flows shows that the main contribution to the energy flux is created by the charged particles of the buffer gas. We also presented for comparing results of heat flux when the HCM was supplied by high power impulse magnetron sputtering (HiPIMS) source.

Keywords: Hollow cathode magnetron, energy flux, HiPIMS, Langmuir probe.

1. Introduction

Hollow cathode magnetrons (HCMs) are the plasma sources used for film deposition using metal atoms and ions. The HCM's cup-shaped target geometry electrostatically and magnetically confines electrons within the volume of the source so that losses are minimized. The characteristic difference between this technique and conventional approaches is that high fractions of the sputtered material is ionized, while in traditional magnetron sputtering, the sputtered species are almost exclusively neutral. Magnetic field is directed along a sidewall surface of the magnetron and has a cusp at the mouth of the cathode. Magnetic field captures secondary electrons emitted from the cathode, which produce an ionization of the buffer gas and sputtering atoms of the target. Crossed ExB fields cause electron drift in an azimuthal direction, in result inside the hollow cathode plasma of high density (> 10^{12} cm^{-3}) is created.

These sources produce plasma with a density of more than 10^{11} cm^{-3} in a large volume. The substrate is set from the source at a distance of 15-20 cm in order to increase the ionization probability of the sputtered atoms on their way from the target to the substrate. The high-ionized metal flux allows the film to be deposited submicron patterned structures with high aspect ratio (ratio of depth to width). In particular, these sources are used to create the adhesive, diffusion and seed layers in the trenches and vias of modern VLSI [1-4]. Preparation of films in such sources is stimulated by a large flow of ions, which allows to obtain nanostructured films with unique properties.

Questions of plasma interaction with a solid surface are extremely important for a wide range of technological applications, such as the deposition of thin films and modification of various surfaces. The energy flux of incoming particles (electrons, ions and neutrals), infrared radiation and the resulting surface temperature determine many processes such as adsorption, diffusion and chemical reactions. Ultimately, the microstructure and hence properties of the obtained films depend on energetic conditions at the surface.

The energy flux to a substrate is a key parameter in sputtered thin film deposition and many researchers have measured it by using thermal probes (TPs) in various processing plasmas

[5-20]. However, to our knowledge, measurements of the energy flux of the HCM have not been performed.

In this paper, experimental results of the spatial distributions of the total energy flux q_{total} and the partial energy fluxes q_x due to plasma charged and neutral species in the deposition zone are presented. Using the data obtained the energy flux composition of q_x in the HCM sputtering is discussed. A high plasma density in the HCM increases the contribution of charged particles to the energy flux in contrast to conventional magnetrons, where the essential contribution is created by the target material atoms [7-11]. HCMs have been investigated both experimentally and via computer modeling [1-4, 21, 22], but many phenomena remain unclear.

The purpose of this work is to study the energy flux and its components on a substrate in plasma of HCM, working on DC and high power impulse mode. To solve this problem spatial distribution of energy flux and plasma parameters was measured using energy flux sensor, Langmuir probe and optical emission spectroscopy technique.

1. Experimental apparatus

The experimental setup of the magnetron discharge with a hollow cathode is shown in Fig. 1a [22]. The cathode consists of a cup-shaped Cu target (diameter 0.14 m, length 0.11 m) made of copper and cooled with water. Plasma from the cathode diffuses into a reactor (30 cm diameter, 45 cm length). The electrically insulated insert 200 mm diameter and 110 mm in length is located between the cathode and plasma chamber to create a potential difference with respect to HCM. The chamber was pumped to base pressure 10^{-4} Pa using a turbomolecular pump. Argon is used as the buffer gas. Pressure within range of 0.53 - 1.33 Pa was measured using Baratron pressure gauge. Gas flow (25-50 sccm) is provided by the gas flow controller. The magnetic field is produced by eighteen columns of Nd-Fe-B magnets surrounded the target with ring iron flanges on the edges. The magnetic field on the axis is 400 Gs, near the cylindrical surface of the cathode is 450 Gs.

The downstream of the HCM is located the electromagnet. Its magnetic field is opposite in polarity to a magnetic field produced by permanent magnets. In consequence, magnetic field has a cusp at the mouth of the cathode. Plasma stream exits the cathode as a narrow core on the axis. When the

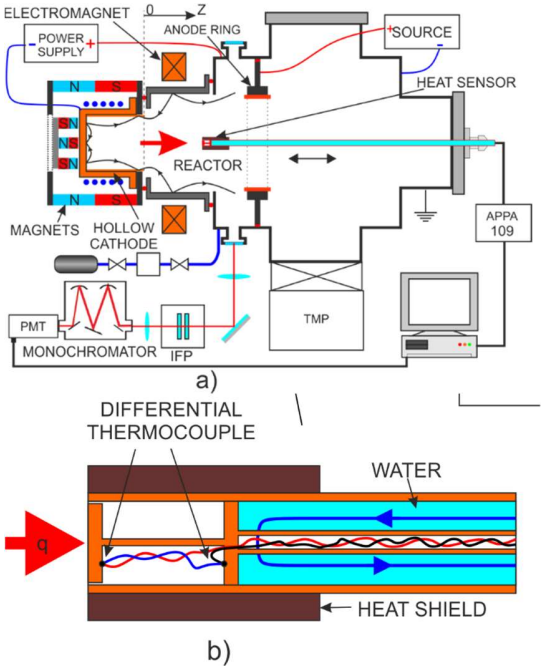

Fig.1. The experimental apparatus – (a) and a scheme of the thermal probe – (b).

electromagnet is on the plasma flow expends to more a uniform radial distribution.

The anode of discharge is a copper ring positioned in the reactor and insulated from it. In the experiments described below, a voltage U_{an} of +30 V was applied to the ring anode from additional source; in this case, the anode collected the entire discharge current.

We used two power sources for HCM: DC inverter source up to 12 kW (20 A, 600 V) and home-made a high power pulse supply capable of delivering 900 V and 150 A peak values.

The main results are given for DC power source. We also present the preliminary results of energy flux when the HCM was supplied by high power impulse magnetron sputtering (HiPIMS) source. In this work, we used discharge with pulse duration of 150 - 300 μs and a repetition frequency of 100 Hz, the duty cycle was equal to 1.5-3%. The pre-ionization system with direct current 5-25 mA and voltage up to 2 kV was used to improve discharge repeatability. The discharge voltage and current were measured by a high voltage probe (P39258, Holden Electronics) and a current sensor CSNB121 (Honeywell) respectively and were recorded by a two-channel digital oscilloscope Bordo 421 (150 MHz).

The energy flux q_{probe} (W/cm^2) was measured by the probe which is shown in Fig. 1b. The substrate of the heat sensor is copper disc diameter of 14 mm and thickness of 5 mm. The middle part (substrate holder) is a copper rod diameter d = 2 mm and length L= 43 mm. The end part is a water-cooled copper cylinder with a diameter of 16 mm and a thickness of 5 mm. The substrate is heated and, after a certain time, it reaches a thermal equilibrium state. At this point the energy flux from the plasma to the substrate q_{in} equals the energy flux from loss processes q_{out} . By neglecting the radiation and convection, q_{out} consists of the heat conduction along the sample holder. Then [9]:

$$q_{prob} = q_{in} = q_{out} \approx \frac{T_S - T_H}{L}, \qquad (1)$$

where T_S is the temperature of the substrate surface, T_H is the temperature at the end of the holder.

The Chromel-Copel thermocouple was glued to the substrate and the rear cylinder through an electric non-conductive adhesive. The probe was closed by a copper pipe ID of 16 mm thickness 1 mm and 40 mm diameter tube from materials having a thermal conductivity of 0.12 W/(m·K) at t = 1100° C for thermal and electric insulation. The calibration of the heat probe was done in vacuum by means of an electrical heater of known power. The energy flux of 1 W/cm^2 corresponds to a temperature difference of about 45^{0}C, so that heat losses by radiation may be neglected. The signal from thermocouple was measured by a multimeter APPA 109.

The heat sensor was installed on the axis of the chamber and can move along it. It was isolated from the ground and thus was at a floating potential. Discharge parameters were quite changed when the sensor was installed at a distance less than Z = 14 cm from the edge of the cathode. (Z = 0 is the output cross section of the cathode). Therefore, the results of measurements at smaller distances are not present.

The electron temperature T_e, electron energy distribution function (EEDF), floating probe potential V_f and plasma potential V_s were determined from probe measurements. We used a flat probe diameter of 2 mm and a cylindrical probe (r = 0.1 mm, l = 2 mm) to measure the plasma parameters along the axis of the discharge. The *I–V* characteristics were recorded with the help PCI card National Instruments NI PCI-6221 with a 16 bit ADC, a 16 bit DAC and multiplexer.

The plasma potential and electron energy distribution function (EEDF) *f(E)* are calculated from the first and second derivatives of the *I-V* curve of a probe respectively. The second derivatives of the probe *I–V* curve were obtained by numerically differentiating the measured *I–V* curves and the electron energy distribution function (EEDF) was given from the Druyvesteyn formula [23].

Due to the influence of magnetic field on the electrons, plasma density was determined from the ion saturation current. The charged particle density n_i was obtained from the saturated ion density current j_i, by using Bohm equation [23]: This can be justified when the ion mean free path is significantly larger than the Debye length, the electron temperature T_e is much greater than the ion temperature T_i. These conditions are correct for the high electron density in our experiment

$$j_i = 0.6 e n_i \sqrt{\frac{kT_e}{M_i}}, \qquad (2)$$

where *e,* M_i and k are the electron charge, ion mass and the Boltzmann constant respectively.

Ion density was calculated by using Sheridan theory [24]. The Sheridan theory considers an increase of geometric probe surface due to sheath. This is taken into account in calculating the ion current density.

No doubly charged ions are observed. Since the probe is located in bulk plasma, the plasma is quasi-neutral there and therefore the electron density is equal to the ion density. The ion density is the ion argon density as the copper ion density is an order of magnitude smaller.

The electron effective temperature T_e is determined as mean kinetic energy of electron gas:

$$T_e = \frac{2}{3} \frac{\int_0^\infty E f(E) dE}{\int_0^\infty f(E) dE} \qquad (3)$$

Here, E is the kinetic energy of the electron gas.

Using plasma parameters obtained, we can determine the contributions from charged particles to the total power density.

For impulse regime of HCM a home-made sample-and-hold system was developed for time-

resolved Langmuir measurements. This system allows to measure the I-V characteristic of the probe in the different stages of a pulsed discharge. The detailed discussion of these measurements is a subject of another article. In this article, we present only some of the results.

Temperature of copper and argon atoms was determined from the Doppler half-width line with a pressure scanned Fabry-Perot interferometer (FPI).

The deposition rate was measured using a quartz crystal microbalance (QCM) an industrial Inficon sensor. The ionization fraction of the copper flux was obtained with QCM in front of which two grids were installed [21].

2.Results

Figure 2a presents measured energy flux as a function of a distance from the magnetron. The energy flux decreases when the distance from magnetron rises. The energy supplied to the surface decreases as the pressure rise. A similar result was obtained by Cormier *et al* [12]. Moreover, the energy flux depends also on the magnetic field configuration.

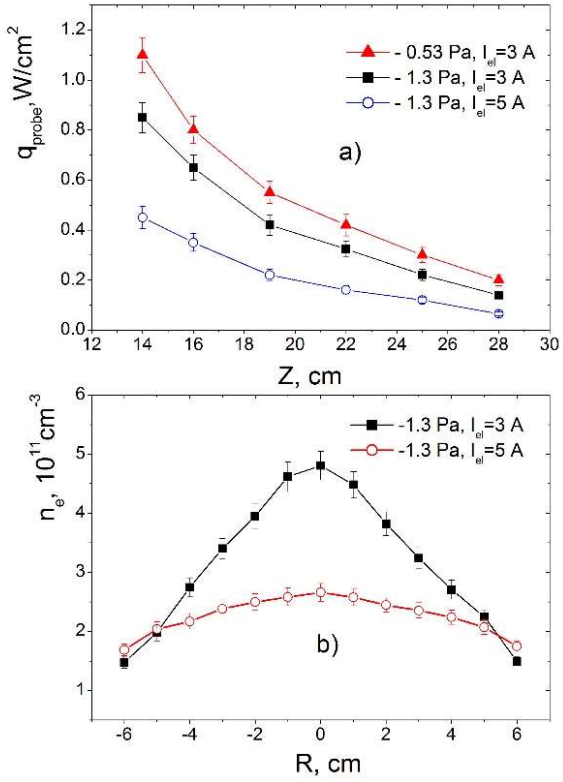

Fig.2. a) Energy flux along Z axis at various pressures and current of electromagnet; b) radial profiles of the electron density n_e. W=2.1 kW, Z =19 cm.

At the same discharge pressure flux decreases when the current of an electromagnet I_{el} rises. The electromagnet changes the geometry of the magnetic field at the outlet of the cathode (Fig. 2b). Plasma has large radial nonuniformity at I_{el} = 3 A [21]. At I_{el} = 5 A uniformity increases but the magnitude of plasma density on the axis is reduced by two times resulting in a decrease of energy flux. Figure 3 shows the dependence of energy flux on the discharge power obtained by sensor installed at a distance of 19 cm from the cathode.

It can be seen that the heat flux increases with decreasing pressure and depends close linear on the discharge power. The Langmuir probe measurements showed that the plasma density increases linearly with the discharge power. These measurements and also the data in Fig. 2b indicate that the major contribution in the heat flux is created by the charged particles.

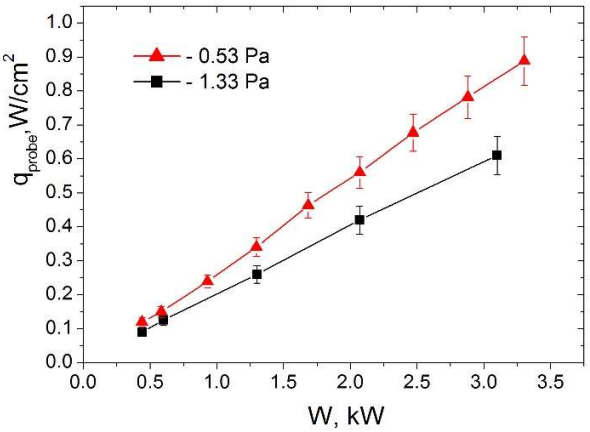

Fig.3. Energy flux versus the discharge power at a distance of 19 cm. I_{el} =3 A.

From the Figure 3 it follows that about 10% of the discharge power is converted into substrate heating. The obtained value is similar to the results of other studies [13].

Figure 4a presents the longitudinal distribution of the electron density n_e, measured at the discharge axis. The electron density falls with increasing the distance. In addition, plasma density increases with pressure growth. We note also that the plasma density exceeds 10^{11}cm^{-3} in the region from 14 to 28 cm.

Floating potential V_f increases by 13 V at a pressure of 0.53 Pa when the distance changes from 14 to 28 cm. At a pressure of 1.33 Pa this increase

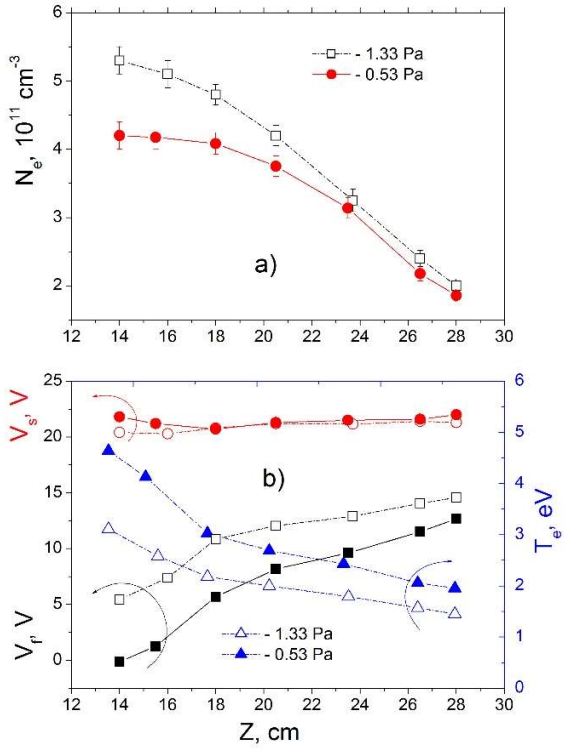

Fig.4. a) Electron density n_e – (a), floating V_f and plasma V_s potentials and electron temperature T_e – (b) versus the distance from magnetron. U_{el} = 3 A, R = 0, W=2.1 kW.

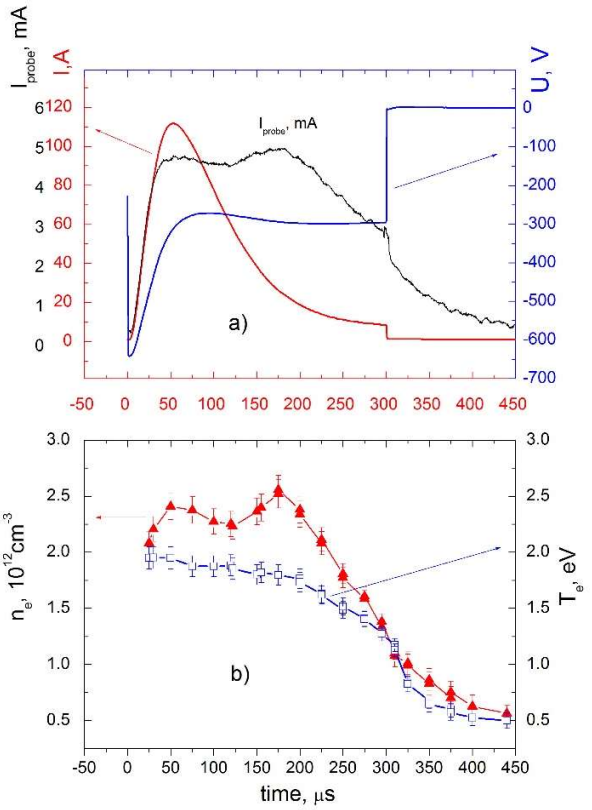

Fig.5. Discharge current, voltage and ion saturation current of the probe – (a), electron density n_e and temperature T_e – (b) as a function of time. HiPIMS discharge, τ = 300 μs, 1.33 Pa, 19 cm, W = 4.23 J, P_{imp} = 14.1 kW, P_{mean} = 423 W.

is 9 V. Plasma potential V_s varies slightly with the distance.

At 0.53 Pa the electron temperature T_e reduces rather steeply from 4.8 eV at Z = 14 cm to 3 eV at 18 cm further decreases more slowly to 2 eV at 28 cm (Fig. 4b). At a pressure of 1.33 Pa the electron temperature is less but the dependence is similar to the previous.

In Fig.5a is shown the typical current and voltage traces from the HiPIMS discharge with pulse duration of 300 μs. The discharge power averaging over the pulse (300 μs) P_{imp} is equal to 14.1 kW and the power averaging over the period (10 ms) P_{mean} is 423 W.

Figure 5a shows also the ion saturation current (V_p = – 60 V), when probe is located at Z = 19 cm along the discharge axis. It can be seen that the plasma recombines for a long time after turning off the discharge. Moreover, probe current shows two distinct peaks. First peak is attributed to argon ions produced in the early stages of the discharge by the ionization front generated by the fast electrons crossing the target to the anode ring. The second peak at 175 μs is from the plasma expansion out of the hollow magnetron. The delay in the arrival of the second peak is attributed to the speed of diffusion through the gas. The temporal evolution of spectral line of Ar ions has also two peaks at 50 μs and 170 μs, whereas the emission of the copper ion has only one peak at 180 -185 μs. The metal ions are mainly generated only after the target current has reached high value. A similar effect was observed in HiPIMS discharges with a planar cathode [25-27].

Figure 5b shows the temporal evolution of the electron density and temperature at Z = 19 cm. The density curve correlates well with the ion current curve. Maximum value of plasma density is $2.5 \cdot 10^{12}$ cm^{-3}.

In the early stage of the discharge (20 μs), the electron temperature is of the order of 5 eV (not shown in the figure). Then the electron temperature falls to 2 eV and decreases smoothly during the discharge. When the discharge is off the temperature drop accelerates.

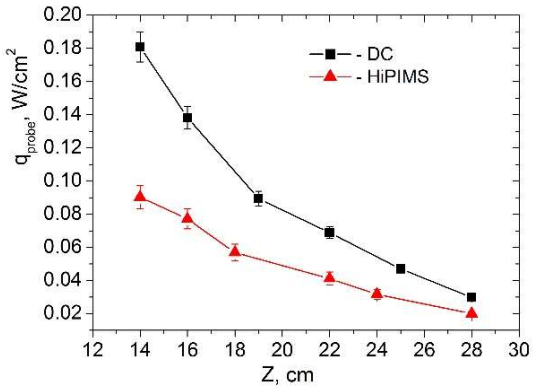

Fig.6. Energy flux as a function of a distance from the magnetron for DC and HiPIMS power supply. I_{el} = 3 A, P = 440 W.

Figure 6 presents measured energy flux density as a function of a distance from the magnetron for DC and a high power impulse supply at $P_{DC} = P_{imp.\,mean}$= 440 W. It is seen that the energy flux in HiPIMS is reduced approximately two - fold.

4. Discussion

In our HCM plasma with the highest density is located near the cylindrical surface [22]. Here magnetic field captures secondary electrons emitted from the cathode, which produce an ionization of the buffer gas and sputtering atoms of the target. Crossed ExB fields cause electron drift in an azimuthal direction, in result inside the hollow cathode plasma near the side surface are generated the high-density plasma.

The plasma parameters obtained from probe measurements are used for a calculation of the different contributions, which sum up to the total energy influx. The power density flux to the sensor (energy flux per time and area) can be represented as follows [9]:

$$q_{total} = q_i + q_e + q_n + q_{rec} + q_{rad}, \qquad (4)$$

Here q_i, q_e are the powers transferred by ions and electrons respectively, q_n is the contribution of neutral species of the buffer gas and the sputtering metal atoms, q_{rec} is energy influx density due to recombination of ions at a surface, q_{rad} is the energy influx due to radiation.

In general, the energy transferred to the substrate is determined by the particle flux density and the mean kinetic energy of the particles. For ions, the mean kinetic energy is mainly given by the difference between plasma potential V_s and the potential of the probe V_f. Thus, the energy influx of ions can be written as [9]:

$$q_i = 0.61 n_e \sqrt{\frac{kT_e}{M_i}} e(V_s - V_f), \qquad (5)$$

The contribution originating from the kinetic energy of electrons (assuming a Maxwellian EEDF) is equal to [9]:

$$q_e = n_e \sqrt{\frac{kT_e}{2\pi m_e}} \exp\left(-\frac{e(V_s - V_f}{kT_e}\right) 2kT_e \qquad (6)$$

The contribution from the recombination process at a floating surface is given by [9]:

$$q_{rec} = j_i \varepsilon_{ion}, \qquad (7)$$

where j_i is the ion flux density and ε_{ion} is the ionization energy.

The energy flux due to neutral atoms consists of thermalized and nonthermalized atoms of the buffer gas and metal. Nonthermalized buffer gas atoms formed because of recombination in collisions of gas ions to the cathode and as a result of resonance charge transfer. Number of the high-energy reflected argon neutrals depends on the reflection coefficient R_N of Ar ions at the target. Eckstein and Biersack [28] study the ion reflection coefficient and the mean energy E_R of reflected atoms. Their calculations for argon shown that R_N = 0.03 and E_R was about average energy of the sputtered particles. Their energy is close to the initial voltage level and hundreds of electron volts.

The kinetic energy of the sputtered metal atoms described by the theory of Thomson, which has a maximum at half of the surface binding energy and the average energy, is about ten electron volts. Since the heat flux sensor (and the substrate) is located at a distance more than 14 cm from the magnetron, then at a pressure of p = 1.33 Pa reflected and sputtered atoms towards the substrate undergo multiple collisions, and thus density of nonthermalized atoms decreases substantially. In addition, in a magnetron with a hollow cathode sputtering takes place on the cylindrical surface of the cathode that is perpendicular to the probe surface [22]. Therefore, the sputtered metal atoms and gas atoms reflected upon recombination of the ions move in a complex path before reaching the substrate. At the same time in the planar magnetron, the substrate is

parallel to the cathode at a close distance. In this case, most of the sputtered target atoms and reflected buffer gas atoms have a preferential direction on the substrate, thus creating an essential contribution to the heat flux. The above arguments also apply to secondary electrons. However, in HCM at a pressure of 0.53 Pa the energy flux of nonthermalized atoms may be significant albeit its value is difficult to calculate.

The energy flux of thermalized buffer gas can be expressed by the following equation [9]:

$$q_n = 0.25 n_{Ar} \sqrt{\frac{8kT_{Ar}}{\pi M_{Ar}}} kT_n \qquad (8)$$

The contribution to the heat flux of the sputtered copper atoms and ions can be determined from measurements of the deposition rate and ionization fraction. The particle flux of the neutrals Γ_n can easily be extracted from measurements of the growth rate R by using $\Gamma = \rho R/m$, where m and ρ denote the mass of the atom and the density of the film, respectively. The deposition rate and ionization fraction were equal to 1.7 nm/s and 25% at the distance of 19 cm from the cathode, discharge power of 2.1 kW and pressure of 1.33 Pa [21]. The temperature of Ar (λ = 750.4 nm) and Cu (λ = 327.4 nm) atoms at a distance of 19 cm increased linearly with the discharge power. At a pressure of 1.33 Pa the temperature of Ar and Cu atoms is equal to 1000 ± 150 K (< 0.1 eV) at a discharge power of 2.1 kW. The flow of atoms and ions of copper at these conditions is approximately $j_{Cu} \approx 10^{16}$ s^{-1}·cm^{-2} and $j_{Cu+} \approx 3 \cdot 10^{15}$ s^{-1}·cm^{-2} respectively. These values are dozens of times less than the flow of atoms and ions of the buffer gas. Thus, the contribution of the kinetic energy of sputtered copper ions and atoms in the heat flux can be neglected.

The energy flux due to condensation of copper atoms can be estimated by [9]

$q_{cond} = j_{Cu} E_{cond}$,

where E_{cond} = 3.2 eV is the condensation energy of copper. The ionization energy of copper atom $E_{rec\ Cu}$ is equal to 7.7 eV. Due to the small fluxes of copper atoms and ions, the values of E_{cond} and $E_{rec\ Cu}$ are several units of mW/cm^2.

Plasma radiation heating at low discharge pressure is small. Detailed analysis of the radiation flux from resonance argon lines in a discharge with the same pressure and with similar plasma density shows that this flux is approximately 5% of the total flow to the substrate [8].

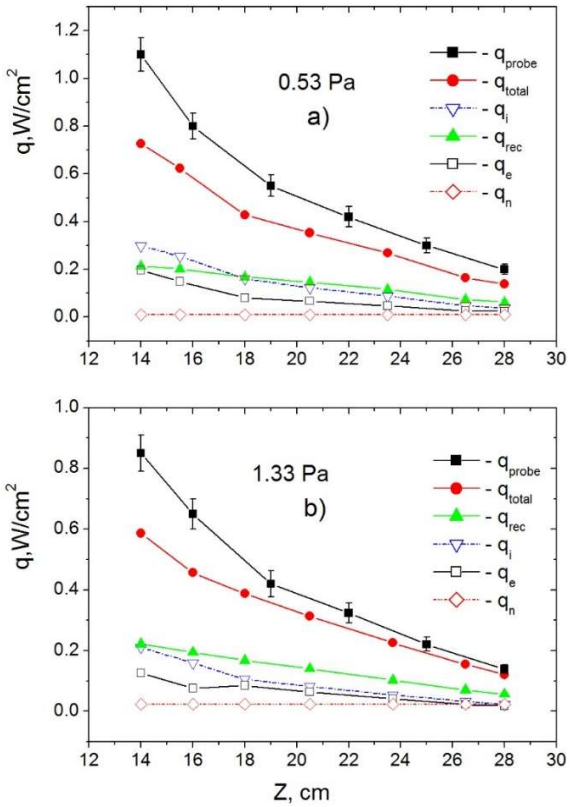

Fig.7. Calculated contributions to the integral energy influx towards the substrate. I_{el} = 3 A, W = 2.1 kW.

Figure 7 a,b show the calculated contributions to the total energy influx towards the probe q_{total} for pressure of 0.53 and 1.33 Pa respectively. It is seen that the main contribution to the energy flux is created by the charged particles of the buffer gas. The energy flux increases with decreasing pressure despite the fact that the plasma density is greater at the higher pressure. Higher electrons temperature in the discharge at low pressure increases the accelerating potential (V_s-V_f) close to the sensor and compensates the adverse effect of density decline.

This figure shows also the measured energy flux q_{probe}. For 1.33 Pa measured flux exceeds the calculated one at about 15% at large distances. Closer to the target, this difference increased to 30%. For 0.53 Pa measured flow exceeds calculated one greater than 30%. We attribute this difference in part to IR from the target and the

insulated insert, which is not water-cooled [18]. As well, the nonthermalized sputtered target atoms and reflected buffer gas atoms can give an appreciable contribution to the energy flux at a pressure of 0.53 Pa.

As stated above the energy flux in the discharge HiPIMS less than DC. A similar result was obtained for a planar cathode [12-14]. Lundin *et al* [13] explained this effect by anomalous transport of high energetic ions in radial direction. In our case, a similar effect can also take place. It can be noted a significant increase in the Cu and Cu+ spectral lines intensity with respect to the Ar lines in our HiPIMS discharge. This indicates growth metal content in plasma. Probably, in the HiPIMS discharge the contribution of sputtered atoms and ions to the energy flux cannot be neglected. Note also that the current density on the target is less than 250 mA/cm^2. Such current density is insufficient for the appearance of self-sputtering. This can be seen from the form of the discharge current. In the emission spectrum of the plasma, there are no lines of doubly charged ions. As is known, doubly charged ions can have high energy [29]. Therefore, in our opinion, the main contribution to the heat flux in pulsed discharge is made by the single-charged ions and electrons. We suppose that the energy flux decline in the HiPIMS discharge can be caused by a decrease in the electron temperature due to an increase of sputtered metal atoms. The energy of the charged particles arriving at the substrate is proportional to the electron temperature.

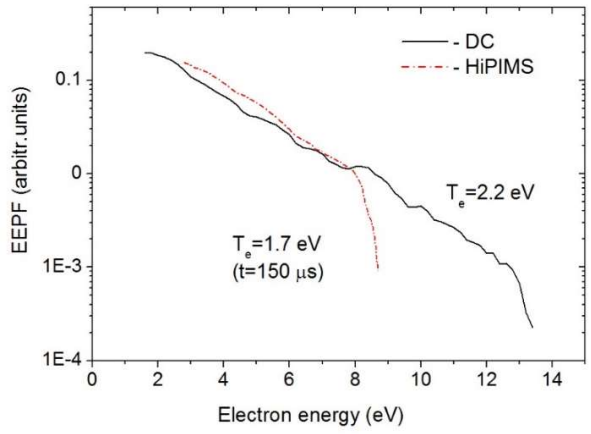

Fig.8. Normalized electron energy probability function at Z = 19 cm. p = 1.33 Pa, I_{el}=3 A, W = 440 W.

Figure 8 presents on the logarithmic scale the electron energy probability function (EEPF) obtained at distance of 19 cm from the cathode. This function is convenient because, for a Maxwellian distribution, its logarithm depends linearly on the electron energy [23]. The slope of the line is defined as $-1/kT_e$ and can be used to calculate the effective electron temperature. As can be seen in DC discharge the energy distributions roughly agree with Maxwellian up to 13 eV. Beginning from 13 eV the EEPF is sharply truncate due to the inelastic (excitation and ionization) electron collisions with argon atoms. In HiPIMS discharge the EEPF is truncate at an energy of 8 eV due to an increase in the sputtered metal atoms. The electron temperature drop reduces the energy flux. The contribution to the energy flux of high-sputtered metal ions observed in HiPIMS discharge with a planar cathode decreases in HCM because of their thermalization due to greater distance to the substrate. A detailed discussion of the reasons for this result requires further study.

5. Conclusion

Axial distribution of the energy flux to a floating substrate in the hollow cathode magnetron discharge was studied at pressures of 0.5 and 1.3 Pa using a thermal probe. We used two power sources for HCM: DC and HiPIMS. As a result, at a distance greater than 20 cm from the target flux density is equal to hundreds mW/cm^2 for DC power supply of 2.1 kW. The energy flux increases linearly with discharge power and depends strongly on magnetic field geometry. For DC discharge, the contribution by charged and neutral species was evaluated from plasma parameters measured by Langmuir probe, FPI and QCM respectively. The energy flux increases with decreasing pressure due to higher electrons temperature. The experimental results were in good agreement with a model based on energy flux calculations due to charge carriers. The energy flow is reduced in HiPIMS by half compared to DC, which, in our assumption, is associated with a decrease in the electron temperature. The main contribution to the energy flux as in DC and in pulsed discharge is created by the charged particles. The maximum temperature reached at the substrate position was found to be

very low for the HiPIMS discharge making it suitable for coating thermally sensitive substrates.

Acknowledgment

This work was supported by a grant from the governor of the Moscow region.

References

[1] E.Klawuhn, G.C.D'Couto, K.A.Ashtiani et al., Ionized physical-vapor deposition using a hollow-cathode magnetron source for advanced metallization, J. Vac. Sci. Technol. A18 (2000) 1546-1549.
[2] L. Meng, R. Raju, R. Flauta, H. Shin, D. N. Ruzic, *In situ* plasma diagnostics study of a commercial high-power hollow cathode magnetron deposition tool, J.Vac.Sci.Technol. A28 (2010) 112 - 118.
[3] L. Wu, E. Ko, A. Dulkin, K. J. Park, S. Fields, K. Leeser, L. Meng, D. N. Ruzic, Flux and energy analysis of species in hollow cathode magnetron ionized physical vapor deposition of copper, Rev. Sci. Instrum. 81 (2010) 123502.
[4] A. Dulkin, E. Ko, L. Wu, I. Karim, K. Leeser, K. J. Park, L. Meng, D. N. Ruzic, Improving the quality of barrier/seed interface by optimizing physical vapor deposition of Cu film in hollow cathode magnetron, J.Vac.Sci.Technol. A 29 (2011) 041514.
[5] J. A. Thornton, Substrate heating in cylindrical magnetron sputtering sources, Thin Solid Films 54 (1978) 23-31.
[6] R.Wendt, K. Ellmer, K. Wiesamann, Thermal power at a substrate during ZnO: Al thin film deposition in a planar magnetron sputtering system, J. Appl. Phys. 82 (1997) 2115-2122.
[7] K. Ellmer, R. Mientus, Calorimetric measurements with a heat flux transducer of the total power influx onto a substrate during magnetron sputtering, Surf. Coat. Techn. 116 (1999) 1102-1106.
[8] R. Piejak, V. Godyak, B. Alexandrov, N. Tishchenko, Surface temperature and thermal balance of probes immersed in a high density plasma, Plasma sources, Sci.Technol. 7 (1998) 590-598.
[9] H. Kersten, H. Deutsch, H. Steffen, G. M. W. Kroesen, R. Hippler, The energy balance at substrate surfaces during plasma processing, Vacuum 63, (2001) 385-431.
[10] H. Kersten, E. Stoffels, W. W. Stoffels, M. Otte, C. Csambal, H. Deutsch, R. Hippler, Energy influx from an rf plasma to a substrate during plasma processing, J. Appl. Phys. 87 (2000) 3637-3645.
[11] M.Cada, J.W.Bradley, G.C.B. Clarke, J.Kelly, Measurement of energy transfer at an isolated substrate in a pulsed dc magnetron discharge, J.Appl.Phys. 102 (2007) 063301.
[12] P.-A. Cormier, A. Balhamri, A.-L. Thomann, R. Dussart, N. Semmar, J. Mathias, R. Snyders, S. Konstantinidis, Measuring the energy flux at the substrate position during magnetron sputter deposition processes, J. Appl. Phys 113, (2013) 013305.
[13] D. Lundin, M. Stahl, H. Kersten and U.Helmersson, Energy flux measurements in high power impulse magnetron sputtering, J. Phys. D: Appl. Phys. 42 (2009) 185202.
[14] G.West, P.Kelly, P.Barker, A. Mishra, J. Bradley, Measurements of deposition rate and substrate heating in a HiPIMS discharge, Plasma Process. Polym. 6 (2009) S543-S547.
[15] M. Wolter, M. Stahl, H. Kersten, Spatially resolved thermal probe measurement for the investigation of the energy influx in an rf-plasma, Vacuum 83 (2009) 768-772.
[16] R. Wiese, H. Kersten, G. Wiese, R.Bartsch, Energy influx measurements with an active thermal probe in plasma-technological processes, EPJ Techniques and Instrumentation 2 (2015) 1-10.
[17] L. Bedra, A. L. Thomann, N. Semmar, R. Dussart, J. Mathias, Highly sensitive measurements of the energy transferred during plasma sputter deposition of metals, J.Phys. D: Appl. Phys. 43 (2010) 065202.
[18] P-A. Cormier, A-L. Thomann, V. Doliqui, A. Balhamri, R. Dussart, N. Semmar, T. Legas, P. Brault, R. Snyders, S. Konstantinidis, IR emission from the target during plasma magnetron sputter deposition, Thin Solid Films 545 (2013) 44-49.
[19] Y. Matsuda, K. Mine, S. Wakiyama, and M. Shinohara, Measurement of energy flux to a substrate by thermal and Langmuir probes during inductively coupled plasma assisted DC

magnetron sputtering, Jap. J. Appl. Physics 54 (2015) 01AB02.
[20] S. Bornhold, H. Kersten, Transient calorimetric diagnostics for plasma processing, Eur. Phys. J. D 67 (2013) 176.
[21] Yu. P. Tsar'gorodtsev, N. P. Poluektov, I. I. Usatov, A. G. Evstigneev, I. A. Kamyschov, Ionization fraction of the sputtered metal flux in a hollow cathode magnetron plasma, Physics Reports 40 (2014) 754-759.
[22] N.P. Poluektov, Yu.P. Tsar'gorodsev, I.I. Usatov, A.G. Evstigneev, I.A. Kamyschov, Plasma parameters of the hollow cathode magnetron inside and downstream, Plasma sources Sci.Technol. 24 (2015) 035009.
[23] M. A. Lieberman, A. J. Lichtenberg, Principles of Plasma Discharges and Materials Processing, Wiley New York, 1994.
[24] T. E. Sheridan, The plasma sheath around large discs and ion collection by planar Langmuir probes, J. Phys.D: Appl. Phys.43 (2010) 105204.
[25] K. Macák, V. Kouznetzov, J.M. Schneider, U. Helmersson and I. Petrov, Ionized sputter deposition using an extremely high plasma density pulsed magnetron discharge, J. Vac. Sci. Technol. 18A (2000) 1533-1737.
[26] A. Vetushka, A.P. Ehiasarian, Plasma dynamic in chromium and titanium HiPIMS discharges, J.Phys.D: Appl.Phys. 41 (2008) 015204.
[27] H Yu, L Meng, M. M. Szott, J. T. McLain, T. S. Cho, D. N. Ruzic, Investigation and optimization of the magnetic field configuration in high-power impulse magnetron sputtering, Plasma Sources Sci. Technol. 22 (2013) 045012.
[28] W. Eckstein, J. P. Biersack, Self-sputtering and reflection, Z.Phys.B Condens. Matter 63 (1986) 109-120.
[29] C. Maszl, W. Breilmann, J. Benedikt, A.Keudell, Origin of the energetic ions at the substrate generated during HiPIMS of titanium, J.Phys.D: Appl.